PROCESSING AND ANALYSIS OF POLARIMETRIC GROUND PENETRATING RADAR LANDMINE SIGNATURES

Friedrich Roth[a], Piet van Genderen[a], Michel Verhaegen[b]
[a]International Research Centre for Telecommunications-transmission and Radar (IRCTR)
[b]Control Laboratory
Faculty of Information Technology & Systems, Delft University of Technology
P.O. Box 5031, 2600 GA Delft, The Netherlands
f.roth@irctr.tudelft.nl p.vangenderen@irctr.tudelft.nl m.verhaegen@its.tudelft.nl

ABSTRACT

This paper presents an analysis of landmine signatures acquired with a polarimetric ground penetrating radar (GPR). First, preprocessing was applied to isolate the target signatures from other reflection events. This included a frequency-wavenumber (*f-k*) filter to remove unwanted side reflections, followed by background subtraction to remove the direct wave and the ground reflection. The obtained polarimetric signatures of the landmines indicated that these can contain significant cross-polar components, which is in contrast to expectation for a target with a cylindrical casing and most likely a result of internal structure. Making use of the reciprocity property of the scattering matrix, the polarimetric signatures were transformed into the target frame, yielding signatures that are independent of target orientation. From the transformed signatures target impulse responses were estimated using a newly developed deconvolution algorithm. The novelty of the deconvolution algorithm lies in the fact that it computes impulse responses, which adhere to a physical model. Accordingly, the computed impulse responses can be related to mine properties such as size and dielectric permittivity. An interesting application of this is the estimation of a mine's permittivity from its impulse response and the impulse response of a calibration target, of which an example is given.

Key words: polarimetric ground penetrating radar, landmine signature, scattering matrix, target impulse response, deconvolution

INTRODUCTION

One of the main objectives of a landmine detection sensor is target identification in order to reduce the false alarm rate. GPR provides a target signature, which contains information on the size, shape and material properties of the target being sensed and can be used for identification. In general, the radar signature of a surface-laid or buried object depends on the orientation of the object with respect to the transmitting and receiving antennas. Consequently, in order to make identification possible, it is necessary to measure the target scattering matrix, which describes the polarimetric scattering behavior of the target. Besides allowing for the transformation of the target signature into an orientation independent coordinate frame, knowledge of the polarimetric scattering behavior provides additional information about the identity of the target.

In this paper, we analyze target signatures of buried landmines measured with a polarimetric GPR. All major aspects of the problem are addressed, from data acquisition to the computation of target impulse responses for identification. Intermediate steps include preprocessing to remove unwanted reflections from the data and the transformation of the measured signatures into an orientation independent coordinate frame. Various examples are given to illustrate the properties of the target signatures and the data processing.

DATA ACQUISITION

The data was acquired over the sandlane of the test facility for landmine detection systems at TNO [1]. The lane contains different types of antipersonnel mines buried at three depths (+1, -1 and -6 cm)[1] and a number of buried false alarms and calibration targets. In this study, we focused on the signatures of three types of mines, a construction brick and a circular metal plate. In the remainder of this paper these mine types will be referred to as type C, E and F respectively. Their properties and those of the brick and the metal plate are summarized in table 1. The sand in the lane was completely dry, having a relative dielectric permittivity of 2.5 and losses close to zero.

[1] With respect to the top of the mine. Negative values correspond to depths below the ground surface.

For the acquisition we used the fully polarimetric video impulse radar developed at the International Research Center for Telecommunications-transmission and Radar (IRCTR) [2]. Its antenna system consists of two transmitting dielectric wedge antennas and four small receiving loops. The configuration is such that it allows measuring the co- and cross-polar components of the scattered field for two mutually orthogonal transmitting polarizations quasi-simultaneously. In this paper these components are denoted as $s_{xx}(t)$, $s_{xy}(t)$, $s_{yx}(t)$ and $s_{yy}(t)$, where the first index specifies the polarization of the receiving loop and the second index the polarization of the transmitting antenna. Together these four components form the scattering matrix $\boldsymbol{S}(t)$. The waveform of the radiated signal was determined in a separate reflection measurement over a metal sheet and its bandwidth was estimated to cover the range of 790 MHz to 3040 MHz on a -10 dB level. All data were acquired using a 10 ns time window of 512 samples corresponding to a time sampling interval of approximately 20 ps.

Accurate antenna positioning was achieved by using a scanning platform, which was placed over the sandlane. B-scans were taken along the *x*-direction of the platform with a spatial sampling interval Δx of 0.55 cm between A-scans. The spatial sampling interval Δy between B-scans was 3 cm. To reduce the amount of data, we only considered every second A-scan resulting in an effective sampling interval Δx of 1.1 cm. The antennas were elevated 48 cm (transmitting) and 20 cm (receiving) above the sand surface.

PREPROCESSING

This section gives an overview of the preprocessing which had to be applied to the data before target signatures could be selected for further analysis. The preprocessing involved the following steps: 1) amplitude and time scale equalization of the co- and cross-polar channels, 2) low-pass filtering for noise reduction, 3) removal of the reflections from the sidewalls of the sandlane, and 4) background removal. All preprocessing steps were designed carefully to avoid unwanted changes in the target signatures.

The sidewalls of the sandlane lead to strong linear reflection events in the B-scans. These were removed by filtering in the frequency-wavenumber (*f-k*) domain taking into account the aliasing of the data along the *y*-direction (figure 1).

In order to achieve optimal separation of the target signatures from the background, two different background subtraction techniques were tested, which differ in the way they estimate the background. The first estimates the background by applying a moving average window and the second technique fits a low degree polynomial to the data. Both techniques are based on the assumptions that the background is smoothly varying and that the targets are isolated scatterers. Due to the small spacing between the targets (45 cm) and the disturbance of the sand during the burial of the false alarms, the data violated these assumptions, making the choice of the width of the averaging window and the degree of the polynomial crucial. The two background subtraction techniques were implemented in both 1D (along the *x*-direction) and 2D (in the *x-y* plane).

Comparison of the background subtraction results demonstrated a better performance of the moving average approach. The background estimates obtained by polynomial fitting did not sufficiently represent local variations, which were present in the data. Furthermore, it was found that 1D background subtraction worked better than 2D because of its lower susceptibility to amplitude and time drift of the GPR system. All A-scans shown in this paper have been obtained after 1D moving average background subtraction with a window width of 50 samples corresponding to a distance of 55 cm. After this background subtraction, the arrivals of some target signatures were still masked by energy, which from looking at B-scans could be identified as residuals from the ground reflection. These were removed carefully by subtracting a scaled and shifted version of the radiated waveform as shown in figure 2.

EXAMPLES OF LANDMINE SIGNATURES

Single Component Target Signatures

Some examples of co-polar target signatures $s_{xx}(t)$ after preprocessing are given in figure 3. All three types of mines have similar signatures, which differ mainly in magnitude. This can be attributed to the fact that the mines have more or less the same height but different diameters (see table 1). As shown in [3], the magnitude of the radar response of a plastic landmine is directly proportional to its cross-section, which agrees with our observation. In contrast, the signatures of the brick and the metal plate differ not just in magnitude but also in shape.

One of the main problems in the quantitative analysis of target signatures is the presence of clutter, which can disturb part of the signature. An example of this is given in figure 3f showing a cluttered type F mine signature. The mine is still visible, though completely mixed with the clutter.

Polarimetric Target Signatures

Figure 4 shows the polarimetric target signature of a type C mine. It is important to note the relatively strong cross-polar components in spite of the mine's cylindrical casing. These cross-polar components can most likely be attributed to the presence of the detonator and other internal mine structure. As a result of reciprocity, the two cross-polar components of the target signature are approximately equal, i.e. $s_{xy}(t) \approx s_{yx}(t)$. Accordingly, the scattering matrix $\boldsymbol{S}(t)$ is symmetric and matrix diagonalization can be applied to transform the target signature into the coordinate frame defined by the main scattering axes of the target called the target frame. In the target frame the cross-polar components vanish and the target signature becomes independent of the target orientation [4].

For comparison, the polarimetric signature of the metal plate is shown in figure 5. As expected for a perfectly rotational symmetric target, the cross-polar components of this target signature are close to zero.

DECONVOLUTION OF THE TARGET IMPULSE RESPONSE

From the selected polarimetric signatures we estimated target impulse responses using a modification of the subset selection deconvolution algorithm described in [5]. It was demonstrated in [5] that the impulse responses estimated by this deconvolution algorithm can be used to distinguish between targets and are described by as few as three parameters, which makes them well suited as input to classification schemes.

The algorithm is based on approximate physical models for the far-field axial impulse response $h(t)$ of a circular metal or dielectric disk embedded in a lossless soil. These are

$$h(t) = -\frac{1}{v\sqrt{\pi}} A\delta'(t) \qquad (1)$$

for the metal disk [6] and

$$h(t) = -\frac{\mu_0 v}{4\sqrt{\pi}} A\Delta\varepsilon \left[\delta'(t) - \Gamma\delta'\left(t - 2l/v_{eff}\right)\right] \qquad (2)$$

for the dielectric disk [3]. In both equations A denotes the cross-section of the disk, v is the wave velocity in the soil and $\delta'(t)$ is the delta function derivative, i.e. a differentiation operator. Furthermore in equation (2), μ_0 is the vacuum magnetic permeability, $\Delta\varepsilon$ describes the permittivity contrast between the disk and the soil, l is the height of the disk, v_{eff} is the effective velocity of the wave propagating through and along the surface of the disk and Γ is a scaling factor accounting for the transmission losses at the top surface of the disk. Looking at equations (1) and (2), we see that a disk differentiates the waveform of the incident wave. The deconvolution algorithm makes use of this fact by computing an optimal impulse response consisting of one (metal disk) or two (dielectric disk) delta function derivatives having magnitude h_1 and h_2 respectively and which are separated by *n* time samples. The optimization is achieved by solving a least squares problem, which minimizes the error between the estimated target signature and the measured target signature. When applying the deconvolution algorithm to the target signatures of the penetrable targets (mines and brick) we imposed additional constraints to prevent the algorithm from producing non-physical results. First, we required that $h_1 h_2 < 0$, i.e. the two delta function derivatives must have opposite polarity. Second, solutions that did not fit the first arrival of the target signature were discarded. Third, we required that $|h_1| - |h_2| < 0.8|h_1|$ in order to avoid solutions with an insignificant second delta function derivative. And fourth, we only considered solutions with $n > 15$ corresponding to a traveltime of 0.3 ns.

Before applying the deconvolution algorithm to the polarimetric target signatures as shown in figures 4 and 5, these were windowed to remove energy that is not part of the target signature. Furthermore, the signatures were transformed into the target frame as described in the previous section. The resulting $s_{xx}(t)$ and $s_{yy}(t)$ signatures were averaged and this average signature was then used as input to the deconvolution algorithm together with the radiated signal determined from the metal sheet reflection measurement.

The output of the deconvolution algorithm for various targets is summarized in table 2. We found that for all penetrable targets (mines and brick) the length *n* of the estimated impulse response is about 30. This agrees with the mines (type C, E and F) and the brick having similar heights ranging from 4 cm to 5.6 cm. For all mines the ratio $|h_2 / h_1|$ is smaller than 0.6 with the exception of the type C mine when buried 6 cm deep. In contrast, the impulse response of the brick is characterized by a strong h_2 and a ratio $|h_2 / h_1|$ of about 0.8.

Figure 6 shows examples of target signatures estimated by the deconvolution algorithm for a type C mine, the brick and the metal plate. For comparison the measured signatures are shown as well. The misfit between the estimated and the measured signatures for the mine and the

brick most likely can be attributed to the fact that the deconvolution algorithm models penetrable targets as homogeneous circular dielectric disks. The signature of the metal plate is well modeled by an impulse response, which only consists of one delta function derivative as indicated by the small misfit in figure 6c.

Equations (1) and (2) suggest an interesting way to estimate the relative permittivity ε_r of a buried mine from its impulse response and the impulse response of a metal plate buried at the same depth:

$$\varepsilon_{r,mine} = \varepsilon_{r,soil}\left(1 + 4\frac{A_{plate}h_{1,mine}}{A_{mine}h_{1,plate}}\right). \qquad (3)$$

Using this equation, we estimated the relative permittivity of the type C mine to be about 4.5.

DISCUSSION

For the quantitative analysis of polarimetric GPR signatures of buried landmines the removal of unwanted reflections is of utmost importance. We have presented preprocessing techniques, which remove the direct wave, the ground reflection and reflections from the sidewalls of the test lane. Still, the presence of clutter can be a serious problem (figure 3f) making it difficult to select target signatures for further processing.

The measured polarimetric signatures of the landmines indicated that these can contain significant cross-polar components $s_{xy}(t)$ and $s_{yx}(t)$ (figure 4), which is in contrast to expectation for a target with a cylindrical casing. Consequently, identifying landmines by looking for targets with negligible cross-polar response is not to be recommended. Furthermore, the antenna configuration of the IRCTR video impulse radar was found to be well suited for measuring polarimetric target signatures, which satisfy reciprocity ($s_{xy}(t) \approx s_{yx}(t)$). Because of this property, the target signatures can be transformed into the target frame, which is crucial for obtaining signatures, which are independent of target orientation.

The deconvolution algorithm described in this paper is based on physical models for the impulse response of a buried metal or dielectric disk. This has the advantage that the computed target impulse responses have a physical meaning. A direct application of this is the estimation of the relative permittivity of a mine as given by equation (3).

In general, the impulse responses computed for the three types of mines (C, E and F) showed similar characteristics. They consist of two delta function derivatives, which are separated by about 30 time samples; the first delta function derivative is negative and the second is much weaker than the first and positive. To determine whether this is enough information to distinguish the mines from other targets requires further measurements with more types of buried objects.

ACKNOWLEDGEMENTS

This research was funded by the Dutch Technology Foundation STW, applied science division of NWO. The authors wish to thank Ainhoa Gorriti from the Section of Applied Geophysics, TU Delft, for the laboratory measurement of the dielectric permittivity of the sand from the TNO test lane.

REFERENCES

[1] W. de Jong, H.A. Lensen, and Y.H.L. Janssen, “Sophisticated test facility to detect land mines”, *Proc. SPIE*, vol. 3710, Detection and Remediation Technologies for Mines and Minelike Targets IV, 1999, pp. 1409-1418.

[2] A.G. Yarovoy, L.P. Ligthart, A.D. Schukin, and I.V. Kaploun, “Full-polarimetric video impulse radar for landmine detection”, *Proc. SPIE*, vol. 4758, 9th International Conference on Ground Penetrating Radar, 2002, pp. 246-250.

[3] F. Roth, P. van Genderen, and M. Verhaegen, “Radar response approximations for buried plastic landmines”, *Proc. SPIE*, vol. 4758, 9th International Conference on Ground Penetrating Radar, 2002, pp. 234-239.

[4] P. Farinelli, *Polarimetric radar measurements and analysis of surface-laid mine-like targets*, MSc thesis, Faculty of Electronic Engineering, University of Perugia, Italy, 2002, 94 pp.

[5] F. van der Lijn, *Deconvolution of the impulse response of mine-like targets using ground penetrating radar signals*, MSc thesis, Faculty of Applied Physiscs, University of Twente, The Netherlands, 2002, 98 pp.

[6] S. Nag and L. Peters, “Ramp response signatures for dielectric targets, *Proc. SPIE*, vol. 3392, Detection and Remediation Technologies for Mines and Minelike Targets III, 1998, pp. 703-713.

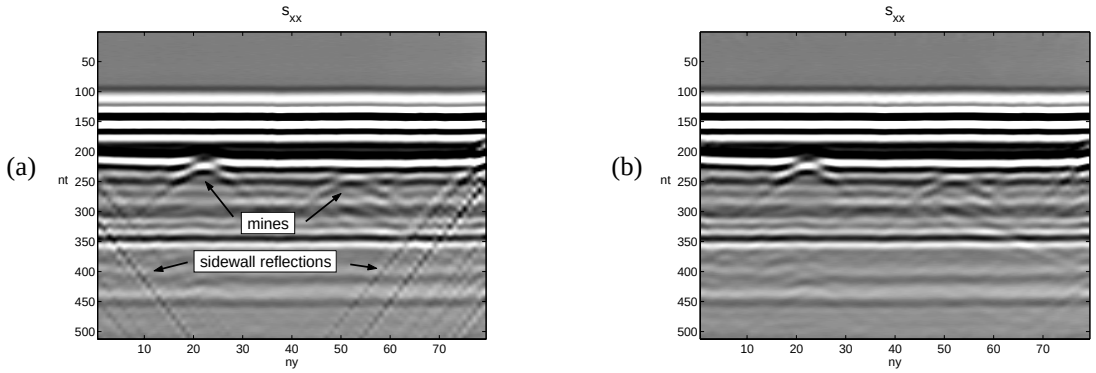

Figure 1: Removal of the sidewall reflections by *f-k* dip filtering: (a) before and (b) after filtering.

Table 1: Target properties.

Target	Shape	Dimensions*	Material
AP mine type C	cylindrical	11.2 cm (d) 5.6 cm (l)	plastic casing; high metal content
AP mine type E	cylindrical	7 cm (d) 5.2 cm (l)	plastic casing; low metal content
AP mine type F	cylindrical	5.6 cm (d) 4 cm (l)	plastic casing; low metal content
metal plate	circular	10 cm (d)	metal
brick	rectangular	15 cm (a) 7 cm (b) 4 cm (l)	construction brick

*d: diameter, l: height, a: length, b: width.

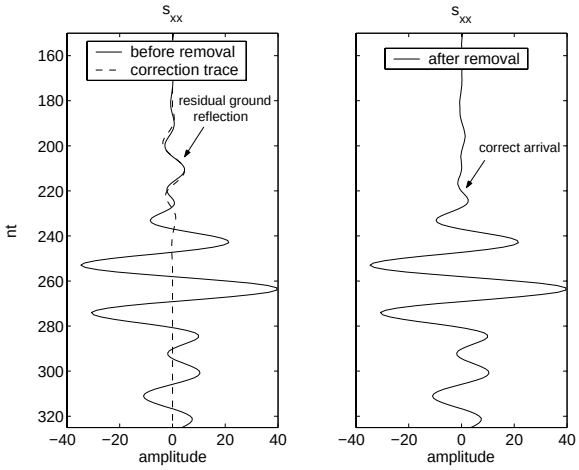

Figure 2: Removal of the residual ground reflection for a type C mine (depth: - 6 cm).

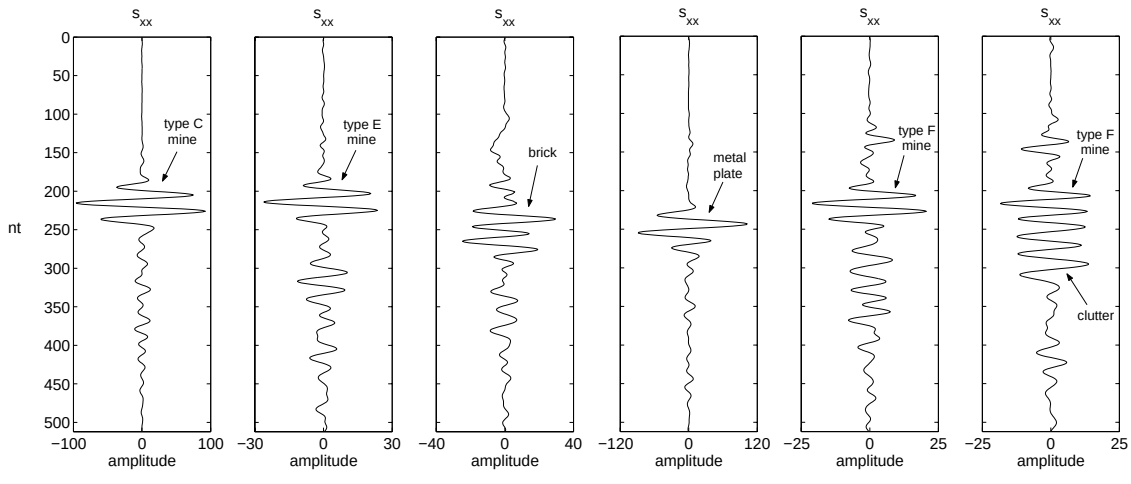

Figure 3: Co-polar target signatures $s_{xx}(t)$ of
(a) a type C mine (depth: +1 cm), (b) a type E mine (depth: +1 cm), (c) the brick (depth: -6 cm),
(d) the metal plate (depth: -6 cm), (e) a type F mine (depth: + 1cm), (f) a type F mine with clutter (depth: +1 cm).

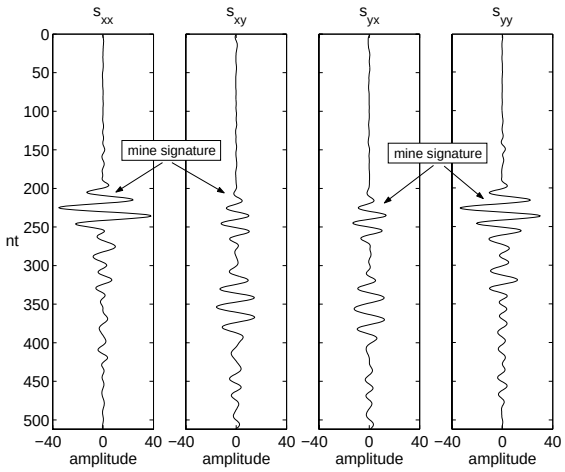

Figure 4: Polarimetric signature of a type C mine (depth: -1 cm).

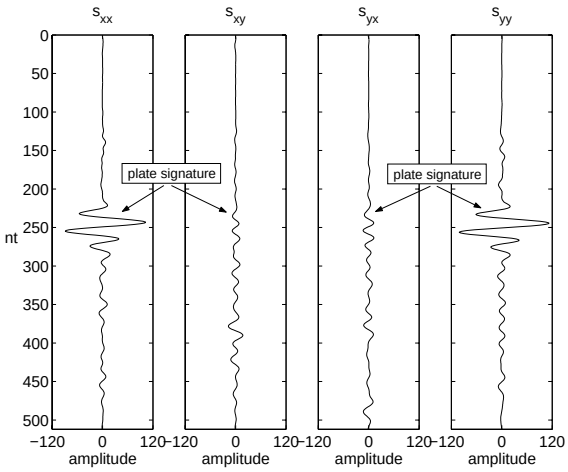

Figure 5: Polarimetric signature of the metal plate (depth: - 6 cm).

Table 2: Deconvolution results.

Target	Depth [cm]	h_1	h_2	n	$\lvert h_2 / h_1 \rvert$
AP mine type C	+1	-0.53	0.21	31	0.40
AP mine type C	-1	-0.19	0.09	30	0.47
AP mine type C	-6	-0.17	0.17	31	1.00
AP mine type F	+1	-0.13	0.07	31	0.54
AP mine type E	+1	-0.16	0.04	33	0.25
metal plate	-6	-0.68	×	×	×
brick	-6	-0.16	0.13	28	0.81

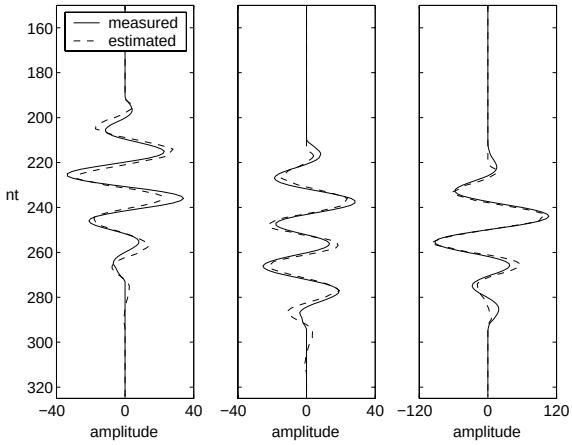

(a) (b) (c)

Figure 6: Measured and estimated (deconvolution) target signatures for
(a) a type C mine (depth: -1 cm),
(b) the brick (depth: -6 cm),
(c) the metal plate (depth: -6 cm).